TEST Engineering & Management

July – August 2020
ISSN: 0193-4120 Page No. 311 - 321

Strain Rate Effect on the Mechanical Properties of Single Coral Particles under Impact Loads

Haotian Zhang[1], Zongmu Luo[1]*

[1]. State Key Laboratory of Disaster Prevention & Mitigation of Explosion & Impact, Army Engineering University of PLA, Nanjing 210007, China

Article Info
Volume 83
Page Number: 311 - 321
Publication Issue:
July - August 2020

Article History
Article Received: *06 June 2020*
Revised: *29 June 2020*
Accepted: *14 July 2020*
Publication: *25 July 2020*

Abstract

Single particle crushing tests have been performed on coral particles with a size range of 5.5-7 mm. A modified split Hopkinson pressure bar (SHPB) apparatus was utilized to achieve impact loads at high strain rates from 103.0 s-1 to 103.5 s-1. Based on the high-speed images, it is found that particle crushing is mainly induced by tensile fracture. The crack initiations of coral particles tend to follow the weak parts at surface defects. Dynamic fragmentation is the ultimate failure feature. The particle crushing strengths were analyzed in terms of survival probability curves, which are proved to follow the Weibull statistics law. The characteristic strength increases with increasing strain rate, which appears to be linear with a slope of 0.385 in the double logarithm coordinate.

Keywords: *Single coral particle; impact load; crushing; strain rate effect*

I. INTRODUCTION

As valuable raw materials, coral aggregates are widely distributed in tropical marine areas such as South China Sea, Red Sea, west continental platform of Australia and Bass Strait. They are commonly used in coastal construction, e.g. building foundations, the backfill material for road embankments, airport runways [1, 2]. In some early offshore engineering projects, geotechnical engineers didn't realize the special characteristics of coral sand, which caused time delays, high costs, and even construction failures [3-5]. Since then, studies on coral sand have been carried out in succession. Coral sand is usually formed by the remains of coral, shells and other ocean creatures through long-term geological processes, with a calcium carbonate content of over 96% [6, 7]. The special formation and composition make coral sand different from traditional terrestrial sand. Compared with quartz sand, coral sand is relatively soft since the Mohs hardness of the main mineral it contains is only half of the former. The porosity ratio of coral sand is higher than that of quartz sand and the inner-pore volume makes up about 10%, further weakening the grain [7]. In addition, stress concentrations occur at sharp edges of coral sand, while quartz sand is well round [6]. As such features above, obvious particle crushing of coral aggregates occurs at a lower stress level. Recently, this phenomenon has aroused general attention.

It is generally believed that particle crushing is the main factor affecting the mechanical properties of coral aggregates. By ring shear and shear box tests, it was found that the stable grading could not be achieved under large deformation due to the breakage of coral sand [8]. Under triaxial shear, the development of grain crushing changes the stress-strain relationship and the dilatancy effect [7, 9]. In the settlement experiment for coral aggregates, unrecoverable relative slips occur between adjacent crushable particles, which eventually cause plastic deformation [6]. Similar features of plastic deformation are shown in single-axial and triaxial compression tests, in which the volume compression is mainly induced by grain crushing [7]. Furthermore, dynamic tests by SHPB indicated that the wave attenuation effect and the energy absorption properties of coral aggregates are better than those of silica sand due to particle crushing and high compressibility [10-12].

The macro-mechanical characteristics of granular aggregates are affected by particle crushing, which is related to the stress environment and individual properties of each single particle. The relationship between the nature of individual particles and the response of the integral material is highly complex. Nakata [13,14] conducted single particle crushing tests on the Aio sand and statistically compared the results with the particle cracking observed in the triaxial test, eventually found that the two results match well. By experimenting with granular materials, they also found that the results of one-dimensional compression test are closely related to the crushing properties of single particles. In the study on granulated coal ash by Yoshimoto [15], the influence of confining pressure on the shear characteristics were examined with the single particle crushing strength taken into account. Shan [16] analyzed the dynamic breakage of single particles of glass sphere, while in Cavarretta's research [17], glass balls were adopted as analogue soil to explore the effects of the mechanical and geometric properties of the particles on the overall cohesionless granular materials. By means of unconventional equipment, Nardelli [18] and Salman [19] analyzed the breakage of Eglin sand particles and spherical alumina particles, respectively.

As above-mentioned, the single particle breakage is one of the prime issues in the study on the mechanical behaviors of granular materials. The mechanical characteristics of single particles can be useful parameters to evaluate those of aggregates. For coral particles, Ma [20] has studied single particle crushing under quasi-static conditions. It was found that the crushing strengths of coral particles accord with Weibull statistical law. The characteristic strength and fracture mode are affected by the loading rate and particle size. However, there are still some issues related to the dynamic mechanical properties of single particle that need to be analyzed in details. Therefore, the present paper places emphasis on the behaviors of single coral particles subjected to impact loads. Dynamic experiments have been performed on individual grains utilizing a modified SHPB equipment. Different strain rates have been obtained by adjusting the value of emission pressure. The instants of particle breakage have been observed via a high-speed camera to investigate the failure modes. By means of statistical methods, the strain rate effect on the single particle crushing strengths have been estimated.

II. SAMPLE PREPARATION

The materials tested are the calcareous coral particles from the Nansha Islands, South China Sea. Samples within the diameter range of 5.5-7 mm have been obtained by sieves, as presented in **Fig. 1**. Scanning Electron Microscopy (SEM) results are also shown in **Fig.1**, indicating that there are many pores distributed around the particle surface. In terms of the widely used reference chart proposed by Krumbein and Sloss [21], specimens with approximately spherical shapes were manually selected.

July – August 2020
ISSN: 0193-4120 Page No. 311 - 321

Sphericity (S) and roundness (R) were adopted to characterize the shape. The PartAn^{3D} particle tracking system was then employed to obtain the shape parameters of the selected particles: the average value of S is 0.902, and the average value of R is 0.487. Some scanning images of particles are exhibited in **Fig. 2**. It indicates that the samples are nearly spherical but not rounded. Before the experiment, particles were cleaned with clear water and placed in a dry ventilated place for one week.

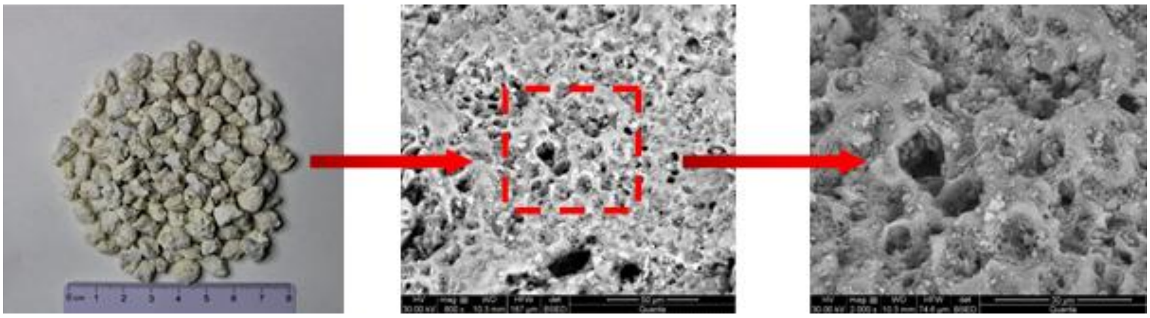

Fig 1. Calcareous coral particles and SEM images.

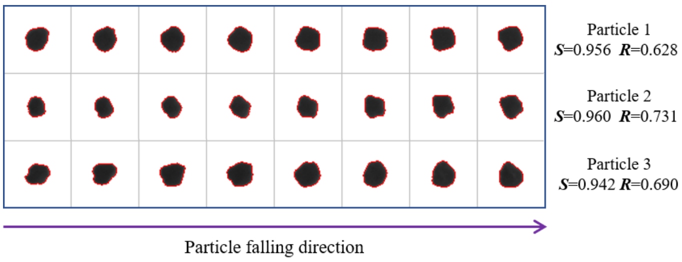

Fig 2. Scanning images of coral particles.

III. EXPERIMENTAL EQUIPMENT AND TESTING PROCEDURES

Split Hopkinson pressure bar (SHPB) apparatus is well-known for characterizing materials at high strain-rates, which was firstly developed by Kolsky in 1949 [22]. In this paper, the dynamic mechanical properties of coral particles have been studied by means of single particle compression tests on SHPB. Considering the gap of impedance between sand material and traditional steel bar, a custom-made low impedance SHPB device was utilized to ensure the accuracy of measurement.

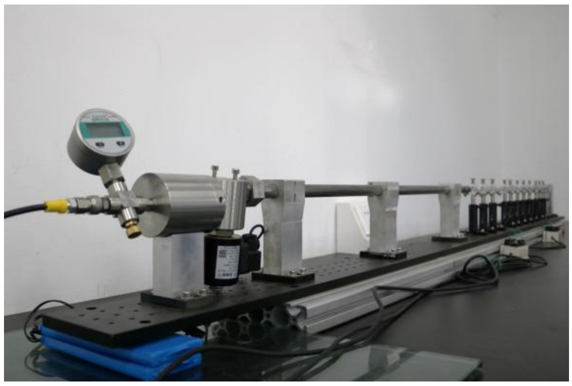

(a) Testing apparatus.

(b) High-speed camera.

TEST Engineering & Management
July – August 2020
ISSN: 0193-4120 Page No. 311 - 321

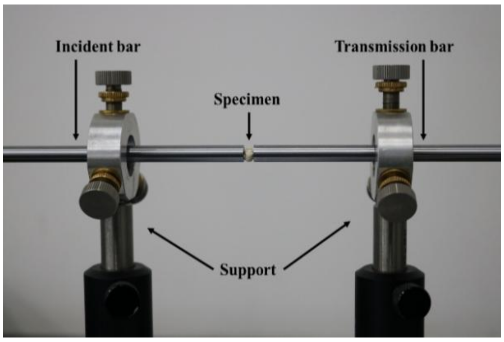

(c) Placement of a specimen.

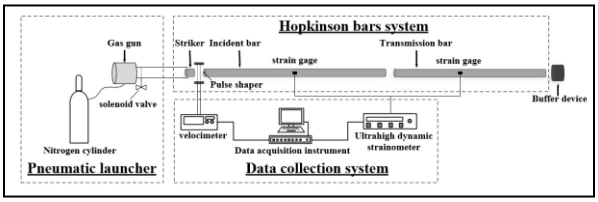

(d) Schematic diagram.

Fig 3. Modified SHPB experimental system.

Real photos and a schematic diagram of the apparatus are presented in **Fig. 3**. The striker, incident bar and transmission bar of the modified device are all made of aluminum rods with a cross section of diameter 6 mm. The lengths are 8 mm, 600 mm and 500 mm, respectively. The elastic modulus of aluminum is 70 GPa and the density is 2700 kg/m^3, which makes its impedance just a third of that of steel. A round piece of rubber (1 mm in thick and 2 mm in diameter) was placed at the center of the end face (close to the striker) of the incident bar. The rubber shaper filters the high-frequency harmonic component of the incident wave and extend the rising time. Hence, brittle coral material would not be damaged at the initial stage of loading, and dynamic loading could be achieved under the of equilibrium stress [23].

Before each single particle crushing test, the particle sample was placed in the most stable direction between the incident bar and the transmission bar. A digital caliper with accuracy of 0.01 mm was used to measure the spacing between the rods, and the result d_0 was taken as the characteristic particle size of the sample. Nitrogen was then filled into the gas gun, and the data collection system was adjusted to ‘waiting to trigger’ state. After connecting the solenoid valve, nitrogen was released from the gas gun instantly and drove the striker to collide with the incident bar. The impact speed was measured via a laser velocimeter, and the loading pulses with different amplitude have been obtained by adjusting the emission pressure in gas gun. The strain gauges were pasted symmetrically to measure the incident signal and reflected signal on the incident bar and the transmitted signal on the transmission bar. The energy carried by the pulse was eventually dissipated at the buffer device. A high-speed camera (FASTCAM SA-Z) and two high-intensity lights were utilized to capture the instant images of the particle breakage. The camera switch was triggered by the incident signal so as not to miss the crushing moment of samples. Five driving pressure levels (650KPa, 670KPa, 690KPa, 710KPa, 730KPa) were adopted to investigate the strain rate effect. 60 repeat tests were conducted under each driving pressure.

IV.Results and analysis

Validation of the SHPB tests

Dynamic compression tests by SHPB have been performed on coral particles. Typical stress wave pulses obtained from strain gages on the incident bar and transmission bar are plotted in **Fig. 4**. Stress equilibrium is considered to be achieved as the difference between the peak value of $\varepsilon_i+\varepsilon_r$ and ε_t is less than one percent of their average peak value, as shown in **Fig. 5**. The engineering load is gained as [22]

$$F(t) = A_t E_t \varepsilon_t(t) \quad (1)$$

where A_t, E_t, ε_t are the cross-sectional area, Young's modulus, strain of the transmission bar, respectively. Strain rate and strain of the specimen are respectively obtained as

$$\dot{\varepsilon}(t) = -\frac{2C_0}{L}\varepsilon_r(t) \qquad (2)$$

$$\varepsilon(t) = \int_0^t \dot{\varepsilon}(\tau)\,d\tau \quad (3)$$

where C_0 is the wave velocity in the bar, ε_r is the strain by the reflected pulse, L is the initial length of the specimen which is equal to the characteristic particle size of the sample (i.e., d_0) mentioned above. **Fig. 6** presents typical strain rate and strain history, and the slope of the straight part of a strain-time history curve is regarded as the dynamic constant strain rate [24].

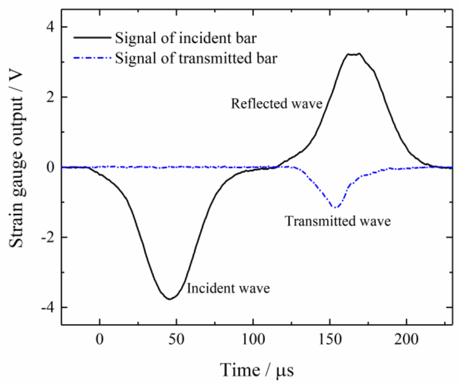

Fig 4. Typical stress wave pulses obtained from strain gages.

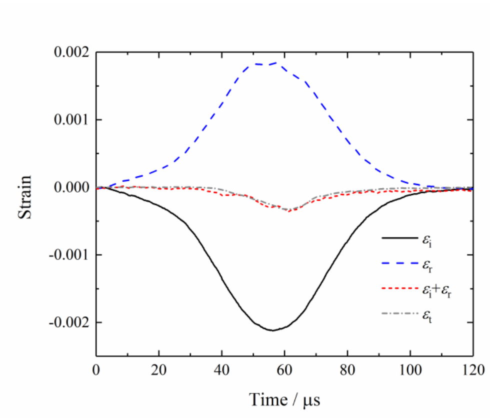

Fig 5. Determination of stress equilibrium by comparing the load at both ends of the specimen.

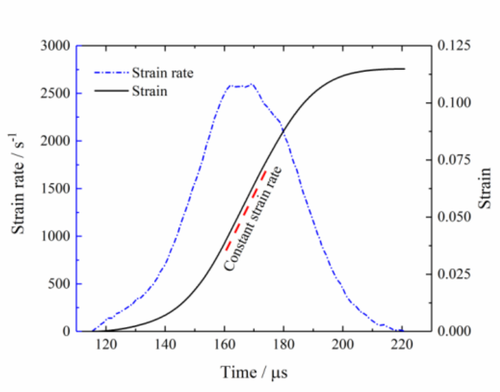

Fig 6. Strain rate and strain history of the specimen.

After impact tests according to the experiment scheme, the test results satisfying the stress equilibrium condition are in **Table 1**. The particle sizes and corresponding strain rates are given. Particles between 5.5 mm and 7 mm have been divided into Group A to Group E according to the strain rates from low to high.

Table 1. Valid experimental results and group classification.

Group	Range of d_0 (mm)	Average of d_0 (mm)	Range of $\dot{\varepsilon}$ (s^{-1})	Average of $\dot{\varepsilon}$ (s^{-1})	Number
A	5.51-6.93	6.15	481-1299	1134	34
B	5.60-6.97	6.05	1302-1598	1430	34
C	5.54-6.99	6.15	1602-1899	1752	38
D	5.51-6.90	6.04	1901-2213	2056	43
E	5.54-6.94	6.10	2215-3519	2574	46

Failure modes of single particles

It is well known that the coral particle is a kind of material with widely distributed internal pores [7], which can be regarded as a crack body containing varying degrees of internal damage. From the microscopic point of view, its dynamic failure is a time process in which different forms

July – August 2020
ISSN: 0193-4120 Page No. 311 - 321

of micro-damage (such as micro-crack, micro-void, micro-shear zone, etc.) evolve at a certain rate [25]. The dynamic crushing processes of coral particles are exhibited in Fig. 7. It can be observed the failure crack of the coral particles is the typical tensile fracture. The crack initiations of coral particles are concerned with the sunken defects present on the surface. As subjected to impact loads, particle samples tend to rupture preferentially along these weak parts. The fracture after initiation is affected by the internal pores and loading rate, and it manifests as different degrees of dynamic fragmentation, i.e., multiple cracks in the material expand at the same time, finally the particle is broken into multiple fragments due to multi-source damage [26, 27].

In addition, it was also found that the strain rate affects the size and number of final fragments. As the strain rate increases, the particles eventually rupture into more finer pieces. The explanation for this phenomenon is relatively mature. The earliest research by Mott [28] on solid fragmentation occurred during World War II. Then Grady and Kip [29] proposed a cohesive fracture model based on Mott's ideas, and concluded that the average fragment size decreases with increasing strain rate. Zhou et al. [30, 31] proposed the Z-M-R model considering a complex dynamic fragmentation mechanism, which obtained similar conclusions.

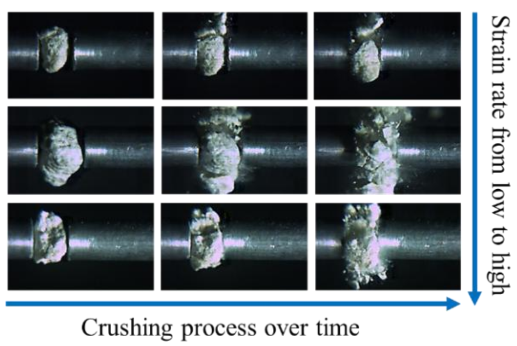

Fig 7. Dynamic crushing of coral particles under high-speed camera.

Dynamic load-displacement curves

Due to the unique structural characteristics of coral particles, such as rough surface, multi-angular and multiaperture, the failure process may be divided into several portions. The angular fracture of the grains causes one or more drops in the load before the final catastrophic rupture, resulting in varied load-displacement relationships. **Fig. 8** shows three typical load-displacement curves of coral particle crushing tests. In **Fig. 8(a)**, the load quickly reaches the peak with an increase in displacement, followed by a sudden decrease as the particle fractures. Such curves generally correspond to samples with smooth surfaces and fewer internal defects, and similar phenomena also occur in quartz sand particle crushing experiments [14]. It can be seen in **Fig. 8(b)** that several small peaks appear before the failure peak appears, which correspond to the slight abrasion and breakage at the edges and corners during the test. With a further increase of load, the overall failure of coral particle occurs. The multi-peak curve in **Fig. 8(c)** shows that the load falls sharply after the first crushing of the particle, soon the remaining specimen contacts the rigid loading surface again. Then the load rises again and usher in a second crushing. The last two relations also come up on crystalline-structure feldspar grains containing incipient flaws [14].

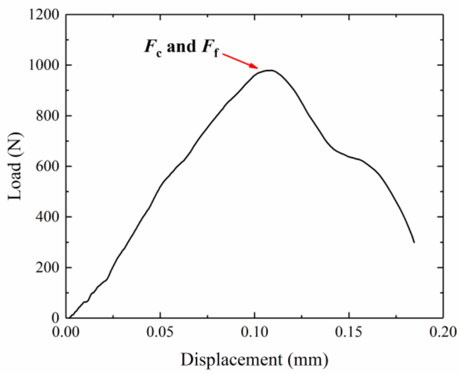

(a)

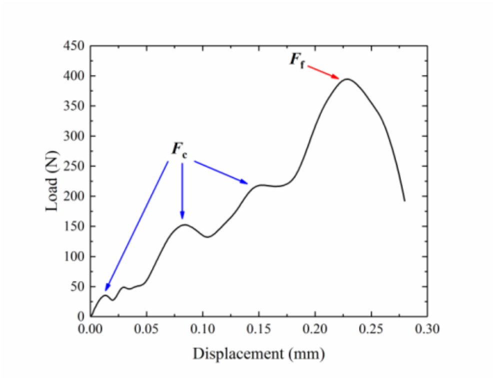

(b)

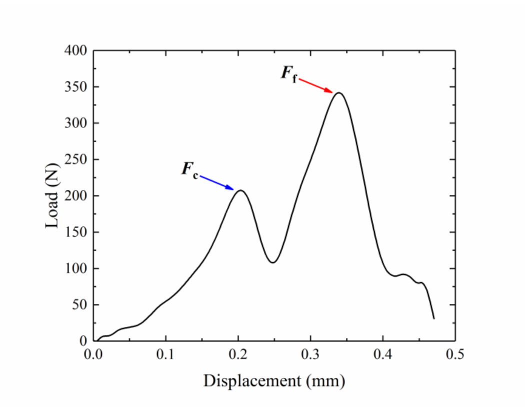

(c)

Fig 8. Typical particle crushing load-displacement relationships.

Effect of strain rate on characteristic strength

The force required to crush a particle can be defined in a variety of ways. In the research of sand particle crushing by Nakata [14], F_c and F_f were defined as the first and maximum peak point where the load declined respectively, and both of the two crushing force were analyzed. In Kwag's investigation for quartz sand and carbonate sand, the first breaking force was used to compare the fragmentation stresses of individual particles [32]. Considering the specialty of the crushing process, Ma [20] regarded the peak force corresponding to the maximum load, F_f, as the critical value when the coral particles split, which is also taken as crushing force in the following analysis.

In each impact test, the loading axis is along the direction of the minimum size of the particle specimen. Based on experimental and theoretical analysis by Hiramatsu [33], the stress state of irregular rocks near the loading axis subjected to concentrated load is roughly the same as that of spherical specimens. The tensile strength of a single particle, σ_f, could be governed by

$$\sigma_f = 1.4\frac{F_f}{2\pi R^2} \approx 0.9\frac{F_f}{d_0^{\ 2}} \qquad (4)$$

Particle crushing strengths are dispersed due to the randomness of particle shape and the inhomogenous distribution of mechanical parameters in particles. Thus, the statistical method proposed by Weibull is adopted to assess the strengths [34]. **Fig. 9** shows the relationships between the survival probability of the particle crushing strength, where the survival probability under a given stress, P_s, is given by **Eq. (5)**.

Experimental results of five groups of particles are presented in **Fig. 9**. It can be seen that particles crushed at higher strain rates have greater probabilities of survival. To facilitate the analysis of tensile strengths of particles, the relationships between survival probabilities and crushing strengths have been described by **Eq. (6)**.

$$P_s = \frac{\text{number of particles with strength greater than } \sigma_f}{\text{total number of particles measured}} \qquad (5)$$

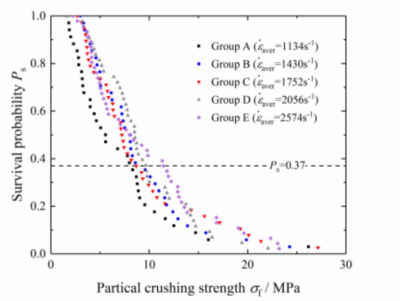

Fig 9. Survival probability curves of different groups of particles.

$$P_s = \exp\left[-\left(\frac{\sigma_f}{\sigma_{f_0}}\right)^m\right] \qquad (6)$$

This is a two-parameter Weibull distribution model, where the characteristic strength, σ_{f0}, is determined as the value of σ_f where P_s=1/e. m is the Weibull modulus related to the variability of strengths in statistics. **Eq. (6)** can be rewritten as

$$\ln\left(\ln\left(1/P_s\right)\right)=m\ln\left(\sigma_f/\sigma_{f_0}\right) \quad (7)$$

The relationships between ln(ln(1/P_s)) and ln(σ_f/σ_{f0}) are plotted in **Fig. 10**. Four sublines are drawn to mark integer values of the Weibull modulus. Results indicate that the data points are in agreement with Weibull distribution, and most of the data is between 1 and 3. The fitted results based on Weibull distribution model are presented in **Table 2**.

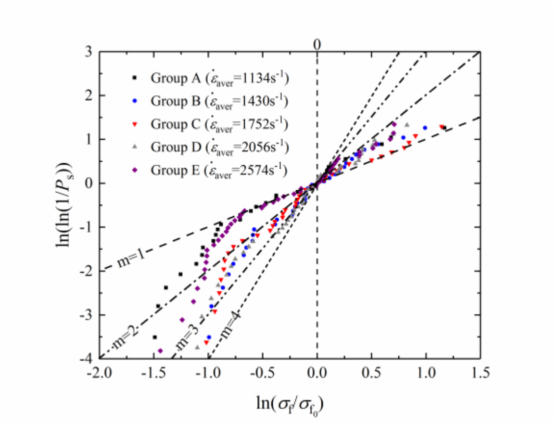

Fig 10. Normalized survival probability curves of different groups of particles.

Table 2 Fitted results of Weibull distribution.

Group	Average of d_0 (mm)	Average of $\dot{\varepsilon}$ (s^{-1})	σ_{f_0} (MPa)	m
A	6.15	1134	8.12	1.397
B	6.05	1430	9.01	2.252
C	6.15	1752	8.65	2.123
D	6.04	2056	9.67	2.412
E	6.10	2574	11.43	1.509

Fig. 11 illustrates the relationships between the characteristic strengths and strain rates in a log-log coordinate. To express the influence of strain rate intuitively, the relations have been fitted as

$$\lg\sigma_{f_0}=a\lg\dot{\varepsilon}+b \quad (8)$$

where a and b are fitted parameters. The fitted line is plotted in **Fig. 11**.

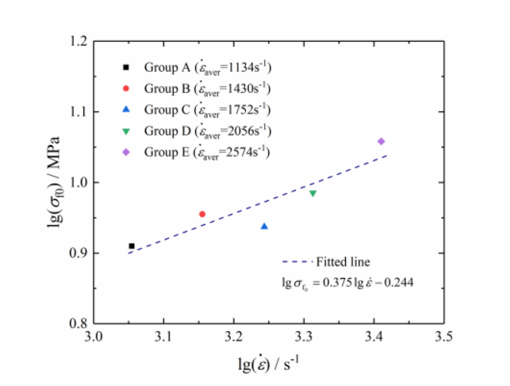

Fig 11. Relationships between the characteristic strengths and the strain rates.

It can be found that the characteristic strengths and strain rates have a linear relationship in the log-log coordinate. The characteristic strength increases in a trend with a slope of 0.375. From the perspective of fracture dynamics [25, 35], the strengths of the coral particle depend on the characteristics of mechanical field near the crack tip and the fracture toughness of the material under impact load. The process of particle crushing can be roughly divided into two steps, i.e., the initial expansion of stable cracks and the propagation and growth of moving cracks. The corresponding critical conditions are governed by

$$K_I^d\left(a,\sigma,t\right)=K_{Id}\left(\dot{K}\right) \quad (9)$$

$$K_I^d\left(a,\dot{a},\sigma,t\right)=K_{ID}\left(\dot{K}\right) \quad (10)$$

July – August 2020
ISSN: 0193-4120 Page No. 311 - 321

V. CONCLUSIONS

Single particle crushing tests have been performed on the coral particles originating from the South China Sea. A low-impedance SHPB device with a diameter of 6 mm was customized to apply impact loads on particles with a size range of 5.5-7 mm. The test results were divided into five groups in terms of the strain rates from low to high. A high-speed camera was utilized to capture the dynamic crushing moment. Results showed that tensile fracture cause particle crushing. The crack initiations are related to the defects on the surface of coral particles. Samples are usually preferentially fractured along these weak parts when subjected to impact load. In addition, dynamic fragmentation is the ultimate failure feature, which becomes more obvious with an increase in strain rate. The crushing strength was calculated based on the maximum load in the load-displacement curve and the characteristic particle size. Survival probability curves and Weibull statistical method were adopted to estimate the strength characteristics. The characteristic strengths are highly dependent on strain rates and have a linear relationship in a double logarithmic coordinate with a slope of 0.385.

DATA AVAILABILITY

All data used to support the findings of this study is available from the first author upon request.

CONFLICTS OF INTEREST

The authors declare that there are no conflicts of interest regarding the publication of this paper.

ACKNOWLEDGEMENT

This work has been financed and fully supported by the National Natural Science Foundation of China (Grant Nos. 51774295, 51808551), which are greatly appreciated by the authors.

REFERENCES

[1] Alba, J. L., and Audibert, J. M. "Pile design in calcareous and carbonaceous granular materials, and historic review." Proceedings of the 2nd International Conference on Engineering for Calcareous Sediments. Vol. 1. 1999.

[2] Ma, L. J., Li, Z., Liu, J. G., et al. "Mechanical properties of coral concrete subjected to uniaxial dynamic compression." Construction and Building Materials 199 (2019): 244-255.

[3] Wees, J. A., and Chamberlin, R. S. "Khazzan Dubai no. 1: Pile design and installation." Journal of the Soil Mechanics and Foundations Division 97.10 (1971): 1415-1429.

[4] King, R. W., Van, H. W. R., Kolk, H. F., et al. "Geotechnical investigations of calcareous soils on the North West Shelf, Australia." Offshore Technology Conference. Offshore Technology Conference, 1980.

[5] McClelland, B. "Calcareous sediments: an engineering enigma." International conference on calcareous sediments. 1988.

[6] Wang, X. Z., Jiao, Y. Y., Wang, R., et al. "Engineering characteristics of the calcareous sand in Nansha Islands, South China Sea." Engineering geology 120.1-4 (2011): 40-47.

[7] Yu, H. "Physical and mechanical properties of coral sand in the Nansha Islands." Marine Science Bulletin-Beijing Then Tianjin-English Edition 8.2 (2006): 31.

[8] Luzzani, L., and Coop, MR. "On the relationship between particle. breakage and the critical state of sands." Soils and foundations 42.2 (2002): 71-82.

[9] Datta, M., Gulhati, S. K. and Rao, G. V. "Crushing of calcareous sands during

July – August 2020
ISSN: 0193-4120 Page No. 311 - 321

shear." Offshore Technology Conference. Offshore Technology Conference, 1979.

[10] Yu, X., Chen, L., Fang, Q., et al. "Determination of attenuation effects of coral sand on the propagation of impact-induced stress wave." International Journal of Impact Engineering 125 (2019): 63-82.

[11] Lv, Y. R., Liu, J. G., and Zuo, D. J. "Moisture effects on the undrained dynamic behavior of calcareous sand at high strain rates." Geotechnical Testing Journal 42.3 (2018): 725-746.

[12] Ma, L. J., Wu, J. W., Wang, M.Y., et al. "Dynamic compressive properties of dry and saturated coral rocks at high strain rates." Engineering Geology (2020): 105615.

[13] Nakata, Yukio, et al. "One-dimensional compression behaviour of uniformly graded sand related to single particle crushing strength." Soils and foundations 41.2 (2001): 39-51.

[14] Nakata, Y., Kato, Y., Hyodo, M., et al. "One-dimensional compression behaviour of uniformly graded sand related to single particle crushing strength." Soils and foundations 41.2 (2001): 39-51.

[15] Yoshimoto, N., Hyodo, M., Nakata, Y., et al. "Evaluation of shear strength and mechanical properties of granulated coal ash based on single particle strength." Soils and Foundations 52.2 (2012): 321-334.

[16] [16] Shan, J., Xu, S., Liu, Y., et al. "Dynamic breakage of glass sphere subjected to impact loading." Powder technology 330 (2018): 317-329.

[17] Cavarretta, I., Coop, M. and O'SULLIVAN, C. "The influence of particle characteristics on the behaviour of coarse grained soils." Géotechnique 60.6 (2010): 413-423.

[18] Nardelli, V., Coop, M. R., Andrade, J. E., et al. "An experimental investigation of the micromechanics of Eglin sand." Powder technology 312 (2017): 166-174.

[19] Salman, A. D., Biggs, C. A., Fu, J., et al. "An experimental investigation of particle fragmentation using single particle impact studies." Powder Technology 128.1 (2002): 36-46.

[20] Ma, L. J., Li, Z., Wang, M. Y., et al. "Effects of size and loading rate on the mechanical properties of single coral particles." Powder technology 342 (2019): 961-971.

[21] [21] Krumbein, W. Christian., and Laurence, L. S. Stratigraphy and sedimentation. Vol. 71. No. 5. LWW, 1951.

[22] Kolsky, H. "An investigation of the mechanical properties of materials at very high rates of loading." Proceedings of the physical society. Section B 62.11 (1949): 676.

[23] Frew, D. J., Forrestal, M. J., and Chen, W. "Pulse shaping techniques for testing brittle materials with a split Hopkinson pressure bar." Experimental mechanics 42.1 (2002): 93-106.

[24] Chen, W., Lu, F., and Cheng, M. "Tension and compression tests of two polymers under quasi-static and dynamic loading." Polymer testing 21.2 (2002): 113-121.

[25] Freund, L. B. Dynamic fracture mechanics. Cambridge university press, 1998.

[26] Grady, D. E. "Local inertial effects in dynamic fragmentation." Journal of Applied Physics 53.1 (1982): 322-325.

[27] Lankford, J. A. M. E. S., and Blanchard, C. R. "Fragmentation of brittle materials at high rates

July – August 2020
ISSN: 0193-4120 Page No. 311 - 321

of loading." Journal of materials science 26.11 (1991): 3067-3072.

[28] Mott, N. F. "A theory of the fragmentation of shells and bombs." Fragmentation of Rings and Shells. Springer, Berlin, Heidelberg, 2006. 243-294.

[29] Kipp, M., and Grady, D. E. "Dynamic fracture growth and interaction in one dimension." Journal of the Mechanics and Physics of Solids 33.4 (1985): 399-415.

[30] Zhou, F. H., Molinari, J. F., Ramesh, K. T. "A cohesive model based fragmentation analysis: effects of strain rate and initial defects distribution." International journal of solids and structures 42.18-19 (2005): 5181-5207.

[31] Zhou, F. H., Molinari, J. F., and Ramesh, K. T. "Effects of material properties on the fragmentation of brittle materials." International journal of fracture 139.2 (2006): 169-196.

[32] Kwag, J. M., Ochiai, H., Yasufuku, N. "Yielding stress characteristics of carbonate sand in relation to individual particle fragmentation strength." Engineering for calcareous sediments 1 (1999): 79-86.

[33] Hiramatsu, Y., Oka, Y. "Determination of the tensile strength of rock by a compression test of an irregular test piece." International Journal of Rock Mechanics and Mining Sciences & Geomechanics Abstracts. Vol. 3. No. 2. Pergamon, 1966.

[34] Weibull, W. "A statistical distribution function of wide applicability." Journal of applied mechanics 18.3 (1951): 293-297.

[35] Ravi-Chandar, K. Dynamic fracture. Elsevier, 2004.

[36] Zhang, Q. B., and Zhao, J. "A review of dynamic experimental techniques and mechanical behaviour of rock materials." Rock mechanics and rock engineering 47.4 (2014): 1411-1478.

[37] Chen, E. P., and Sih, G. C. "Transient response of cracks to impact loads." Mechanics of fracture 4 (1977): 1-58.

[38] Achenbach, J. D. "Dynamic effects in brittle fracture." Mechanics today 1 (1972): 1-57.